Oxidation of H$_2$ and CO over Ion-Exchanged X and Y Zeolites

Daniel G. Lahr, Junhui Li, and Robert J. Davis*

Contribution from the Department of Chemical Engineering, University of Virginia, Charlottesville, Virginia 22904-4741

Received October 5, 2006; E-mail: rjd4f@virginia.edu

Abstract: Zeolites X and Y exchanged with Group IA cations were synthesized by aqueous ion exchange of NaX and NaY and used as catalysts in the oxidation of H$_2$ and CO at temperatures ranging from 473 to 573 K. The CsX zeolite was the most active material of the series for both reactions whereas HX was the least active. Moreover, the oxidation of CO in H$_2$ was very selective (~80%) over the alkali-metal exchanged materials. Isotopic transient analysis of CO oxidation during steady-state reaction at 573 K was used to evaluate the coverage of reactive carbon-containing intermediates that lead to product as well as the pseudo-first-order rate constant of the reaction. A factor of 4 enhancement in activity achieved by exchanging Cs for Na was attributed to a higher coverage of reactive intermediates in CsX because the pseudo-first-order rate constant was nearly same for the two materials (~0.7 s^{-1}). The number of reactive intermediates on both materials was orders of magnitude below the number of alkali metal cations in the zeolites but was similar to the number of impurity Fe atoms in the samples. Because the trend in Fe impurity loading was the same as that for oxidation activity, a role of transition metal impurities in zeolite oxidation catalysis is suggested.

Introduction

Frei recently summarized the rapid progress achieved on the selective partial oxidation of hydrocarbons in faujasite-type zeolites,[1] which has been a growing area of research over the past decade.[2–15] One major difficulty encountered during partial oxidation of hydrocarbons with molecular oxygen is the formation of combustion side products formed at the elevated temperatures typically required for the reaction. Moreover, the higher reactivity of partially oxidized products compared to hydrocarbons exacerbates the problem of low selectivity. New routes to selectively oxidize molecules are clearly needed. Frei et al. discovered that photoactivation of hydrocarbon and dioxygen molecules loaded into a zeolite cage can yield selective oxidation products at relatively low temperatures.[1–6] They suggest the high electric field associated with the charge-balancing zeolite cations lowers the energy required to excite charge transfer from the hydrocarbon to dioxygen. Therefore, excitation by visible light or by mild heating can initiate the oxidation reaction to produce a radical hydrocarbon cation and a superoxide (O$_2^-$) anion. The highly acidic radical cation then transfers a proton to the superoxide to form a hydroperoxide molecule, which decomposes to yield a selective oxidation product.[1] Although this novel approach to selective oxidation avoids the high temperatures typically encountered in oxidation reactions, the microporous nature of the zeolite prevents desorption of the products to complete the catalytic cycle.

Xu et al. followed the selective oxidation of propane to acetone over various ion-exchanged Y zeolites in the absence of irradiation and found the reaction rate increased in the order BaY < MgY < SrY < CaY.[12] In a follow-up study, they studied the same reaction over various Ca-exchanged zeolites and found that activity and selectivity were a function of zeolite type.[13] For example, high selectivity to partial oxidation was observed over CaY whereas deep oxidation of propane to CO and CO$_2$ was observed over Ca-exchanged mordenite, presumably because of Bronsted acid sites present in the latter material. For hydrocarbon oxidation, alkaline-earth exchanged zeolites are generally found to be more active than alkali-metal exchanged zeolites, presumably because of the high electric field associated with divalent cations compared to monovalent cations.[3] Indeed, Xu et al. prepared a series of NaY zeolites containing various levels of ion-exchanged Ca and studied these materials in the selective oxidation of propane.[14] The acetone formation rate correlated well with Ca loading in the zeolite supercages.

A recent quantum chemical study by Pidko and van Santen explored the initial charge-transfer step proposed for selective

(1) Frei, H. *Science* **2006**, *313*, 309.
(2) Blatter, F.; Frei, H. *J. Am. Chem. Soc.* **1993**, *115*, 7501.
(3) Blatter, F.; Sun, H.; Vasenkov, S.; Frei, H. *Catal. Today* **1998**, *41*, 297.
(4) Vasenkov, S.; Frei, H. *J. Phys. Chem. B* **1998**, *102*, 8177.
(5) Frei, H.; Blatter, F.; Sun, H. U.S. Patent 5,914,013, assigned to the Regents of the University of California, June 22, 1999.
(6) Frei, H.; Blatter, F.; Sun, H. U.S. Patent 5,827,406, assigned to the Regents of the University of California, Oct. 27, 1998.
(7) Tang, S. L. Y.; McGarvey, D. J.; Zholobenko, V. L. *Phys. Chem. Chem. Phys.* **2003**, *5*, 2699.
(8) Panov, A. G.; Larsen, R. G.; Totah, N. I.; Larsen, S. C.; Grassian, V. H. *J. Phys. Chem. B* **2000**, *104*, 5706.
(9) Myli, K. B.; Larsen, S. C.; Grassian, V. H. *Catal. Lett.* **1997**, *48*, 199.
(10) Xiang, Y.; Larsen, S. C.; Grassian, V. H. *J. Am. Chem. Soc.* **1999**, *121*, 5063.
(11) Larsen, R. G.; Saladino, A. C.; Hunt, T. A.; Mann, J. E.; Xu, M.; Grassian, V. H.; Larsen, S. C. *J. Catal.* **2001**, *204*, 440.
(12) Xu, J.; Mojet, B. L.; van Ommen, J. G.; Lefferts, L. *Phys. Chem. Chem. Phys.* **2003**, *5*, 4407.
(13) Xu, J.; Mojet, B. L. Lefferts, L. *Micropor. Mesopor. Mater.* **2006**, *91*, 187.
(14) Xu, J.; Mojet, B. L.; van Ommen, J. G.; Lefferts, L. *J. Phys. Chem. B* **2004**, *108*, 15728.
(15) Vanoppen, D. L.; De Vos, D. E.; Jacobs, P. A. *J. Catal.* **1998**, *177*, 22.

photo-oxidation reactions in zeolites.[16] They studied the adsorption and reaction of 2,3-dimethyl-2-butene in a model pore of the Y-zeolite supercage with two alkaline earth cations in appropriate positions. In contrast to earlier studies, they suggest that the electrostatic field of the zeolite pore is not the key feature of the system. Instead, they found the relative orientation and distance between 2,3-dimethyl-2-butene and O_2 to be the important factor. From their perspective, the zeolite pore organizes the reagents into a pre-transition state arrangement via interactions with the exchange cations. This model accounts for CaY being more active that MgY and SrY, because the Ca ions are of the appropriate size in the zeolite cage. The smaller Mg and larger Sr cations did not produce as suitable a configuration of 2,3-dimethyl-2-butene and O_2 as did the Ca cations.

Recent work in our lab revealed that both butane and butene are catalytically oxidized over Cs and Na exchanged X zeolites at moderate (474–573 K) temperatures.[17] However, we observed gas-phase CO_2 without any significant quantity of CO in the product stream. In an effort to better understand oxidation catalysis in zeolites, we decided to explore the steady-state carbon monoxide oxidation and dihydrogen oxidation over alkali-metal and alkaline-earth exchanged zeolites. However, we realize that these steady-state reactions require higher temperatures than those typically used during photo-oxidation reactions in zeolites. Because CO and H_2 oxidation reactions do not form multiple oxidation products, a direct comparison with partial oxidation of hydrocarbons will be limited.

Carbon monoxide oxidation is a very well-studied reaction because of its utilization in automotive emissions control. More recently, preferential oxidation (PROX) of dilute carbon monoxide in dihydrogen streams over zeolite-supported transition metal catalysts has attracted attention for low-temperature PEM fuel cell operations.[18–20] Although PROX is effectively catalyzed by an expensive transition metal such as Pt, a suitable non-transition metal catalyst would be highly desirable.

In this study, we used isotopic transient analysis of the CO oxidation reaction to probe the number of reactive intermediates and the pseudo-first-order rate constant of the oxidation reaction occurring at the steady state. In addition, the rates of dihydrogen oxidation are compared directly to those of CO oxidation over a series of ion-exchanged zeolites.

Experimental Procedures

Catalyst Preparation. Ion-exchanged zeolites were prepared according to methods described previously.[17] In summary, NaX (Union Carbide, lot 07483-36) or NaY (Union Carbide, lot 955089001010-S) was triply ion-exchanged with 1 M aqueous solutions (10 mL g⁻¹ original zeolite) of the appropriate salt. Cesium acetate (Aldrich 99.9%), potassium nitrate (Aldrich 99+%), sodium acetate (Acros 99+%), barium acetate (Aldrich 99.999%), strontium nitrate (Acros ACS grade), calcium nitrate tetrahydrate (Acros ACS grade), and magnesium acetate hexahydrate (Acros 99%) were used as ion precursors. After the ion-exchange steps, each 3 g sample was triply washed with 1 L of distilled deionized water for 5 h. Each sample was then dried overnight in air

at 363 K and calcined at 773 K for 5 h. An HX sample was prepared by ion-exchanging NaX with ammonium nitrate (Acros, 99%) as described above. However, after low-temperature drying, the material was evacuated at room temperature for 2 h and heated under vacuum at 723 K for 5 h to remove ammonia from the catalyst. Elemental composition of these samples, determined by ICP analysis, was performed by Galbraith Labs, Inc. (Knoxville, TN).

Addition of iron to zeolite X was accomplished by sublimation of $FeCl_3$ as described by Chen and Sachtler.[21] Approximately 3 g of zeolite (NaX and HX) was placed on one side of a U-tube and heated under helium flow at 623 K for 2 h. The $FeCl_3$ was placed in the other side of the U-tube, and the entire system was heated to 623 K to sublime iron chloride into the zeolite. The yellow zeolite product was then washed with distilled deionized water and calcined at 773 K for 5 h.

Oxidation Reactions. The zeolite catalyst was loaded into a single-pass fixed bed reactor system operating at atmospheric pressure. Prior to reaction, the catalyst was heated in situ in flowing helium at 773 K for 5 h. The reactant gases CO (BOC 99.997%) and O_2 (BOC, 99.999%) were both purified by passage through a silica gel trap immersed in dry ice acetone, whereas H_2 (BOC, 99.999%) was purified by a Supelco OMI-2 filter. Argon (BOC, 99.999%) and helium (BOC, 99.999%) were purified in sequence by a Supelco OMI-2 filter and a silica gel trap held in dry ice acetone. The oxidation reactions involved 5 mol % H_2 or CO, 2.5 mol % dioxygen, and the balance inert. To improve sensitivity in the thermal conductivity detector, helium was used during carbon monoxide oxidation reactions whereas argon was used during dihydrogen reactions. In some cases, both dihydrogen and carbon monoxide were fed to the oxidation reactor. These PROX conditions were 40 mol % dihydrogen, 5 mol % carbon monoxide, 2.5 mol % dioxygen, and the balance helium. The total flow rate in all cases was 54 mL min⁻¹. Products were monitored with an online gas chromatograph equipped with a Alltech CTR I column and a thermal conductivity detector using helium or argon as the reference gas depending on the inert gas fed to the reactor.

Isotopic Transient Measurements. Approximately 0.3 g of catalyst was loaded into a fixed bed tubular reactor connected directly to a mass spectrometer. The same gases, purification methods, and catalyst pretreatments were used as described above. In addition, ¹³C-labeled carbon monoxide, ¹³CO, (Cambridge Isotopes, 99.5% CO, 98+% ¹⁶O, 99+% ¹³C) was used to evaluate the number of reactive intermediates and the relaxation time of the system. Isotopic transient experiments involving ammonia synthesis and carbon monoxide oxidation have been performed extensively in our lab,[22–27] and the reactor system used in this study is the same as the one used previously. Reaction conditions were 2.5% carbon monoxide, 2.5% dioxygen, 94% helium, and an additional 1% argon or helium. Volumetric flow rates ranged from 160–300 mL min⁻¹. A Balzers-Pfieffer Prisma 200 amu mass spectrometer was used to monitor the concentrations of argon and the carbon dioxide isotopomers, ¹²CO_2 and ¹³CO_2, in the effluent stream.

First, the carbon monoxide reaction was run at the steady state. Then, an isotopic switch in one of the reactants, i.e., ¹²CO/¹³CO, is performed while keeping all other variables constant. Care was taken to keep the pressure constant at 2.6 bar throughout the switch. To account for the gas-phase holdup, an inert tracer (Ar) of 1 mol % was also switched with the carbon monoxide. For more information on the method, see the excellent review of Shannon and Goodman.[28]

(16) Pidko, E. A.; van Santen, R. A. *J. Phys. Chem. B* **2006**, *110*, 2963.
(17) Li, J.; Tai, J.; Davis, R. J. *Catal. Today* **2006**, *116*, 226.
(18) Igarashi, H.; Uchida, H.; Suzuki, M.; Sasaki, Y.; Watanabe, M. *Appl. Catal. A: Gen.* **1997**, *159*, 159.
(19) Watanabe, M.; Uchida, H.; Ohkubo, K.; Igarashi, H. *Appl. Catal. B: Env.* **2003**, *46*, 595.
(20) Rosso, I.; Galletti, C.; Saracco, G.; Garrone, E.; Specchia, V. *Appl. Catal. B: Env.* **2004**, *48*, 195.

(21) Chen, H.-Y.; Sachtler, W. M. H. *Catal. Lett.* **1998**, *50*, 125.
(22) McClaine, B. C.; Davis, R. J. *J. Catal.* **2002**, *210*, 387.
(23) McClaine, B. C.; Davis, R. J. *J. Catal.* **2002**, *211*, 379.
(24) Siporin, S. E.; Davis, R. J. *J. Catal.* **2004**, *222*, 315.
(25) Calla, J. T.; Davis, R. J. *J. Phys. Chem. B* **2005**, *109*, 2307.
(26) Calla, J. T.; Bore, M. T.; Datye, A. K.; Davis, R. J. *J. Catal.* **2006**, *238*, 458.
(27) Calla, J. T.; Davis, R. J. *J. Catal.* **2006**, *241*, 407.
(28) Shannon, S. L.; Goodwin, J. G., Jr. *Chem. Rev.* **1995**, *95*, 677.

Table 1. Unit Cell Composition and Impurity Iron Content of Ion Exchanged X and Y Zeolites[a]

sample	pore volume (cm^3 g^{-1})	unit cell composition	ion exchange (%)	iron loading (ppm)
HX	0.21	$H_{50}Na_{33}Si_{109}Al_{83}O_{384}$	60	176
NaX	0.32	$H_3Na_{80}Si_{109}Al_{83}O_{384}$	96	282
KX	0.25	$H_{13}Na_9K_{61}Si_{109}Al_{83}O_{384}$	73	379
CsX	0.19	$H_6Na_{34}Cs_{43}Si_{109}Al_{83}O_{384}$	52	442
NaY	ND[b]	$H_5Na_{48}Si_{139}Al_{53}O_{384}$	91	ND[b]
CsY	ND[b]	$H_2Na_{14}Cs_{37}Si_{139}Al_{53}O_{384}$	70	204

[a] Protons were added to unit cell compositions to balance framework charge. [b] ND: not determined.

Table 2. Rates of H$_2$ and CO Oxidation over Group IA X and Y Zeolites[a]

	H$_2$ oxidation reaction rate (μmol g^{-1} s^{-1})		CO oxidation reaction rate (μmol g^{-1} s^{-1})	
sample	573 K	473 K	573 K	473 K
HX	0.2	0.10	0.08	0.012
NaX	1.71	0.55	0.14	0.022
KX	2.86	0.92	0.1	0.018
CsX	10.43	1.31	0.44	0.039
NaY	0.4	0.14	0.04	0.006
KY	0.74	0.18	0.06	0.009
CsY	1.78	0.22	0.12	0.010

[a] Operating conditions: 54 mL min^{-1}, 5% H$_2$ or CO, 2.5% O$_2$, balance inert, 0.03 g catalyst for NaX, KX, CsX, and H$_2$ at 573 K, otherwise 0.3 g catalyst.

Results and Discussion

Elemental analysis of the zeolite samples was used to calculate the unit cell compositions shown in Table 1 and confirmed the expected levels of ion-exchange in the zeolites. Because the Cs$^+$ ion has a radius of 1.7 Å, it is too large to exchange with sodium in the sodalite cages. Thus, it is not surprising to see a fairly modest level of Cs exchange in the X zeolite. Pore volumes, calculated as the amount of liquid dinitrogen adsorbed in the zeolite pores at a relative pressure (P/P_o) of 0.3 are also shown in Table 1. The pore volume of the X zeolites decreased as the cation size increased, with the exception of HX. Although it is likely that HX partially degraded during preparation, the reasonably high pore volume indicates the zeolite was mostly intact.

The reaction rates of dihydrogen oxidation and carbon monoxide oxidation over the ion-exchanged zeolites are summarized in Table 2. The reactor was operated at low conversion (under 10%) to ensure the differential behavior. Although a steady state was achieved within 30 min, the reactions were performed for over 4 h.

Several interesting trends were observed in the oxidation of dihydrogen and carbon monoxide over the ion-exchanged zeolites. First, the dihydrogen oxidation rate was much higher than the carbon monoxide reaction rate over all zeolites. The reaction rates were also a strong function of zeolite cation. Dihydrogen oxidation over CsX was over an order of magnitude faster than over HX, whereas the same comparison for CO oxidation shows only a 3−5-fold increase. Moreover, the trend in the dihydrogen oxidation rate was CsX > KX > NaX > HX. Although CsX was the most active catalyst for CO oxidation, there was no clear trend with the other X zeolites. Table 2 also reveals that CsX was about 6 times more active for dihydrogen oxidation than CsY, and KX was about 4 times

Table 3. Rates of H$_2$ and CO Oxidation over Alkaline-Earth Exchanged X Zeolites[a]

	H$_2$ oxidation reaction rate (μmol g^{-1} s^{-1})		CO oxidation reaction rate (μmol g^{-1} s^{-1})	
sample	573 K	473 K	573 K	473 K
MgX	1.23	0.23	0.03	0.005
CaX	0.49	0.26	0.08	0.010
SrX	1.57	0.16	0.1	0.017
BaX	1.84	0.31	0.06	0.009

[a] Operating conditions: 54 mL min^{-1}, 5% H$_2$ or CO, 2.5% O$_2$, balance inert, 0.3 g catalyst.

Table 4. Activity and Selectivity of Alkali-Metal Exchanged X Zeolites during Preferential Oxidation of CO in H$_2$ at 573 K[a]

sample	PROX selectivity[b]	CO oxidation rate (μmol g^{-1} s^{-1})
NaX	81	0.08
KX	77	0.07
CsX	85	0.35

[a] Reaction Conditions: 54 mL min^{-1}, 40 mol % H$_2$, 5 mol % CO, 2.5 mol % O$_2$, balance helium. [b] Defined as (moles of CO$_2$ produced/(2 × moles of O$_2$ consumed)).

more active than KY. In general, the relative rates between the X and Y zeolites averaged to about 5 for dihydrogen oxidation and about 3 for carbon monoxide oxidation. Apparently, the number of zeolite cations influenced the overall oxidation rates because Y zeolites contain fewer of them than X zeolites. The number of accessible cations in Site III positions varies between X-type and Y-type zeolites by a factor of 4.8, and after accounting for Type II sites, the cation ratio is 1.8.

Table 3 summarizes the oxidation activity over alkaline-earth zeolites. In this case, no clear trend in oxidation activity was seen. Moreover, the alkaline-earth zeolites were less active for both CO and H$_2$ oxidation than the corresponding alkali metal analogues, i.e., CsX > BaX, KX > CaX, and NaX > MgX. Although water produced by H$_2$ oxidation may hydroxylate the multivalent cations during reaction, this should not happen during CO oxidation. Prior work in the area of selective hydrocarbon oxidation over zeolites generally reports increased activity for alkaline-earth exchanged zeolites compared to alkali-metal exchanged zeolites because of the larger local electric field created by alkaline earth cations. If the local electric field in the vicinity of the cation were the key feature in determining the oxidation rate, we would expected the rates to follow the trend CaX > NaX > CsX, which is opposite to what we found in this work.

Reactivity results from the preferential oxidation of CO in the presence of excess H$_2$ (PROX) are reported in Table 4. Evidently, the presence of CO greatly inhibits the H$_2$ oxidation rate because the selectivity of the PROX reaction is about 80% to CO$_2$ over the alkali-metal exchanged X zeolites at 573 K and nearly 100% at 473K (not shown). The dihydrogen oxidation activity regains its original level after removing CO from the feed stream for 3 h. The apparent competition of CO with H$_2$ is consistent with a surface-mediated catalytic reaction involving adsorbed CO.

In an effort to quantify the number of reactive intermediates in the zeolite during CO oxidation, we analyzed the isotopic transient of the product CO$_2$ after a switch in the ^{13}C content of the reactant CO. The total flow rate and average CO$_2$ concentration were both varied to explore the influence of
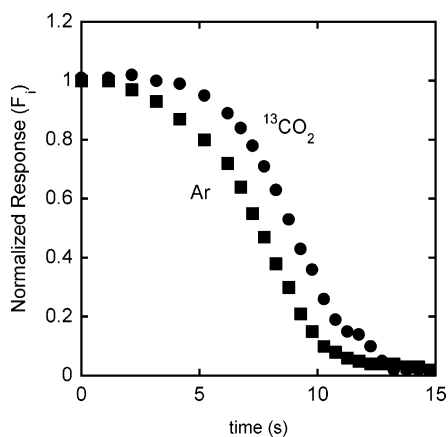
Figure 1. Example of an isotopic transient during CO oxidation over CsX at 573 K.

interparticle and intraparticle readsorption on the observed kinetics. The on-line mass spectrometer used to follow the transient monitored the gas-phase concentration of Ar and the two carbon dioxide isotopomers, $^{12}CO_2$ and $^{13}CO_2$. Because X-type zeolites adsorb significant quantities of water at elevated temperatures, isotopic transients during H$_2$ oxidation were not studied.

The average residence time of surface intermediates that lead to reaction products is found by integrating the normalized transient response after accounting for gas-phase hold-up. This is shown in eq 1.

$$\tau = \int_0^\infty (F_{^{13}CO_2} - F_{Ar})dt \qquad (1)$$

where τ is the mean residence time of reactive carbon-containing intermediates leading to product and F_i are the normalized transient responses of CO_2 and Ar, respectively. Figure 1 shows a typical normalized transient response with Ar and $^{13}CO_2$.

Steady-state oxidation of CO over both CsX and NaX was analyzed using the isotopic transient method. Three flow rates (160, 210, and 300 mL min^{-1}) and three average carbon dioxide concentrations (0.75, 0.95, and 1.2 mol %) were used for nine τ measurements. The overall conversion of CO in our experiments was less than 5%, corresponding to 0.1–0.2 mol % CO_2. Thus, all conditions involved a significant amount of CO_2 co-fed to the reactor to reduce readsorption of the product by competitive adsorption. The residence time τ was evaluated from three measurements of the forward (replacing ^{12}CO with ^{13}CO) and reverse (replacing ^{13}CO with ^{12}CO) switches in feed composition.

A summary of the average τ values obtained from these measurements is shown in Figure 2. The value of τ decreased with increasing flow rate and increasing CO_2 concentration, as expected. The relationship between τ and inverse flowrate indicates *interparticle* readsorption of CO_2 is important. The simplest way to account for interparticle readsorption is to extrapolate the value of τ to infinite flow rate. However, this cannot not correct for *intraparticle* readsorption of product within the catalyst pores. To evaluate the importance of both interparticle and intraparticle readsorption, a similar set of transient experiments was performed without the oxidation reaction. Instead of switching between ^{12}CO with ^{13}CO during CO oxidation, we performed a 0.2 mol % step-change in the CO_2. Although carbon monoxide was not present during the
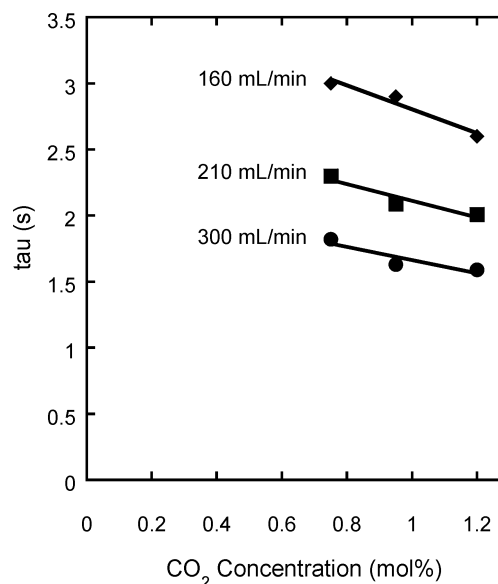

Figure 2. Effect of flow rate and average CO_2 concentration in the reactor on observed relaxation time, τ, over CsX at 573 K. The CO_2 concentration was the average of the inlet and outlet concentrations.
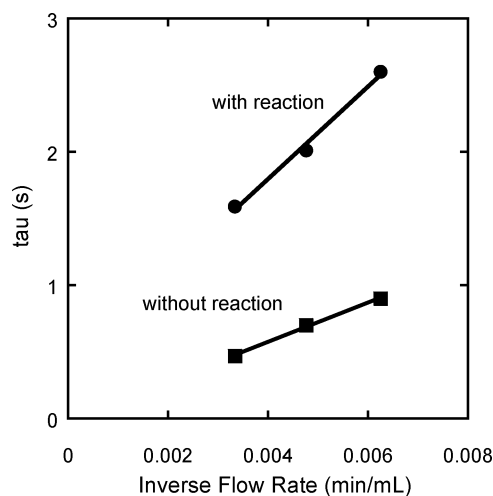

Figure 3. Effect of flow rate on τ at y_{CO2} = 1.2 mol % at 573 K over CsX. "with reaction" indicates data obtained during CO oxidation. "without reaction" indicates CO_2 transient data in the absence of CO oxidation.

switch, all other variables were the same as those in the reactive isotopic transient experiment. The difference between the transient observed during reaction (obtained by switching CO isotopes) and the transient observed without reaction (obtained by a step-change in CO_2 concentration) was attributed to the intrinsic kinetics of the CO oxidation reaction.

Figure 3 shows the results of the switching experiments over CsX zeolite at 573 K, with and without CO oxidation. The upper data set (with reaction) is derived from the three τ values found at 1.2 CO_2 mol % in Figure 2. The lower data set (without reaction) is determined from the CO_2 step-change experiment. The average difference between these two data sets (eq 2) is considered to be the average residence time of carbon-containing reactive intermediates, τ_{intr}.

$$\tau_{intr} = \tau_{w/COrxn} - \tau_{w/outCOrxn} \qquad (2)$$

Equation 3 describes the relationship among τ_{intr}, the number of surface intermediates leading to reaction products, N_{CO2} (mol

g^{-1}), and the overall reaction rate, R_{CO2} (mol g^{-1} s^{-1}).

$$N_{CO_2} = \tau_{intr} \times R_{CO_2} \qquad (3)$$

The pseudo-first-order rate constant, k, of the CO oxidation reaction is simply the inverse of τ_{intr}. Table 5 compares the residence time, rate constant and number of reactive intermediates determined from CO oxidation over CsX and NaX. Although the global rate of CO oxidation varied by almost a factor of 4 between the two catalysts, the intrinsic rate constant was nearly independent of the zeolite cation. The higher rate over CsX is attributed to a higher number of reactive intermediates in the zeolite compared to NaX.

The elemental analysis reported in Table 1 can be used to normalize the coverage of reactive intermediates to the total cation loading of the zeolites or to the iron impurity content in the sample. As shown in Table 5, the number of reactive intermediates is 4–5 orders of magnitude lower than the number of zeolite cations in the samples. An extremely low coverage is also realized when normalizing to only those cations present in the supercages. Interestingly, the coverage of reactive intermediates is between 1 and 10%, when based on the iron impurity level in the zeolite. Moreover, the iron impurity level as provided by Galbraith Labs increases from HX < NaX < KX < CsX, which is the same trend with the activity for H_2 and CO oxidation.

To explore the reactivity of iron in the zeolite, we sublimed FeCl$_3$ into HX and NaX. Iron chloride reacts with protons in the zeolite to form HCl. Because elemental analysis of the NaX catalyst did not show a perfect stoichiometry of Na:Al equal to 1:1, some protons are likely to be present in the sample. After exposure to FeCl$_3$, the NaX turned light yellow-brown in color whereas HX turned very bright yellow, which is consistent with the higher proton content of the latter sample. After washing and calcining the samples, the rate of CO oxidation was evaluated. The oxidation rate of both catalysts was only 30% of the parent material. This decrease in activity could be attributed to pore blockage or to partial deactivation of the active sites by the sublimed Fe. If impurity Fe atoms were the active species in the zeolites, they were in a form that is not readily reproduced by simple iron addition by sublimation. Evidently, Fe must be located in the supercages in an appropriate chemical state to facilitate oxidation catalysis. This conclusion is supported by earlier work with Fe-loaded zeolites. For example, Petunchi and Hall performed a detailed kinetic study of Fe-loaded NaY zeolite containing 6.13×10^{20} Fe atoms per gram of zeolite.[29] From the data presented in that work, the rate of CO oxidation is calculated to be approximately 0.1 μmol g^{-1} s^{-1} at 573 K, which is an order of magnitude greater than the rate over NaY in our Table 2, but less than that over either NaX or CsX. Moreover, the turnover frequency (TOF) of the reaction based on the Fe content over the Fe–NaY prepared by Petunchi and Hall was estimated to be 1×10^{-4} s^{-1} at 573 K, which is several orders of magnitude lower than the value of k reported in Table 5. Because the pseudo-first-order rate constant determined from isotopic transient analysis is considered to be an intrinsic rate at which the catalytic cycle turns over, the low TOF reported by Petunch and Hall was likely the result of very few of the Fe atoms participating in the reaction.

(29) Petunchi, J. O.; Hall, W. K. *J. Catal.* **1982**, *78*, 327.

Table 5. Relative Surface Coverages during Carbon Monoxide Oxidation over Ion-Exchanged X Zeolite as Determined by Isotopic Transient Analysis

parameter	CsX	NaX
τ_{intr} (s)	1.3	1.7
k (s^{-1})	0.77	0.59
N (μmol g^{-1})	0.69	0.23
$\theta_{ion}{}^a$	2.9×10^{-4}	3.9×10^{-5}
θ_{Fe}	0.09	0.03

^{a} Based on total cesium or sodium content in the zeolite.

The results of our study suggest that transition metal impurities may play an important role in zeolite oxidation catalysis. This is reminiscent of the findings by Parmaliana et al., who reported that isolated Fe impurities account for the catalytic activity and high selectivity of commercial silica samples in the partial oxidation of methane to formaldehyde.[30,31] Although there is abundant evidence that hydrocarbon oxidation in zeolites, whether photoassisted or not, is strongly influenced by the presence of alkali metal and alkaline earth cations, a similar conclusion cannot be drawn unambiguously for the oxidation of small molecules such as H_2 and CO. The lower reactivity of alkaline-earth exchanged zeolites compared to alkali-metal exchanged zeolites together with a strong competition of CO with H_2 for active sites during PROX are consistent with a normal surface redox mechanism for the reactions. Indeed, Aparicio and Dumesic have modeled the oxidation of CO over a variety of transition metal-loaded zeolites according to a simple redox mechanism.[32] Therefore, a strong correlation of oxidation activity with alkali metal or alkaline earth cations in zeolites does not by itself justify the role of field effects in oxidation catalysis because the level of transition metal impurities can also vary with cation type.

It should be noted that an Fe impurity level of 300 ppm in zeolite X corresponds to about 1% of the supercages having an associated Fe atom. Interestingly, Vasenkov and Frei used time-resolved FT–IR spectroscopy to study the visible-light-induced oxidation of 2,3-dimethyl-2-butene in NaY.[4] Their elegant experiments utilized a short (150 ms) photolysis pulse to determine the number of supercages involved in the oxidation reaction without the complication of cage-to-cage diffusion of the reactants. They found a minimum of 1% of Y zeolite supercages are involved in the photoreaction, which is far above the estimated level of defects in the zeolite. It is, however, near the transition metal impurity level of some faujasite zeolites as shown in Table 1. Thus, although other evidence supports the idea that zeolite countercations influence hydrocarbon oxidation activity through either an electric field effect or a preorganization of the transition state, there might still be an important role of impurity transition metal ions in other oxidation systems.

Conclusions

The oxidation of H_2 and CO was catalyzed by ion-exchanged X and Y-type zeolites at temperatures ranging from 473 to 573 K. For H_2 oxidation, the reactivity trend was CsX > KX > NaX > HX. Likewise for CO oxidation, CsX was the most active sample and HX was the least active of the Group IA exchanged zeolites. Moreover, oxidation activities of CsX and

(30) Parmaliana, A.; Arena, F.; Frusteri, F.; Martinez-Arias, A.; Lopez Granados, M.; Fierro, J. L. G. *Appl. Catal. A: Gen.* **2002**, *226*, 163.
(31) Arena, F.; Parmaliana, A. *Acc. Chem. Res.* **2003**, *36*, 867.
(32) Aparico, L. M.; Dumesic, J. A. *J. Mol. Catal.* **1989**, *49*, 205.

KX were greater than those of the corresponding Y zeolites, CsY and KY. Comparison of Group IA exchanged zeolite X to Group IIA exchanged samples, i.e., CsX vs BaX, KX vs CaX, and NaX vs MgX, revealed higher activity of the alkali metal forms. The PROX behavior of the Group IA-exchanged X zeolites exhibited a high selectivity ($\sim$80%) of CO oxidation over H_2 oxidation at 573 K. Isotopic transient analysis during steady-state CO oxidation over CsX and NaX suggests the higher activity of CsX results mainly from a higher concentration of reactive intermediates in the sample. Although the coverage of reactive intermediates was many orders of magnitude below the cation loading in the zeolites, it was similar to the iron impurity level in the samples. Because the overall trend in the iron impurity content is similar to the reactivity trend for the reactions studied here, a critical role of iron impurities in the oxidation catalysis cannot be ruled out. It is quite possible, however, that favorable molecular interactions of the reactants with heavy alkali metal cations are responsible for the observed catalysis. This study suggests that future work with oxidation in zeolites should always address a possible role of redox impurities in the catalytic cycle.